

Supplementary Materials

***In-situ* real-time monitoring of muscle energetics with soft neural-mechanical wearable sensing**

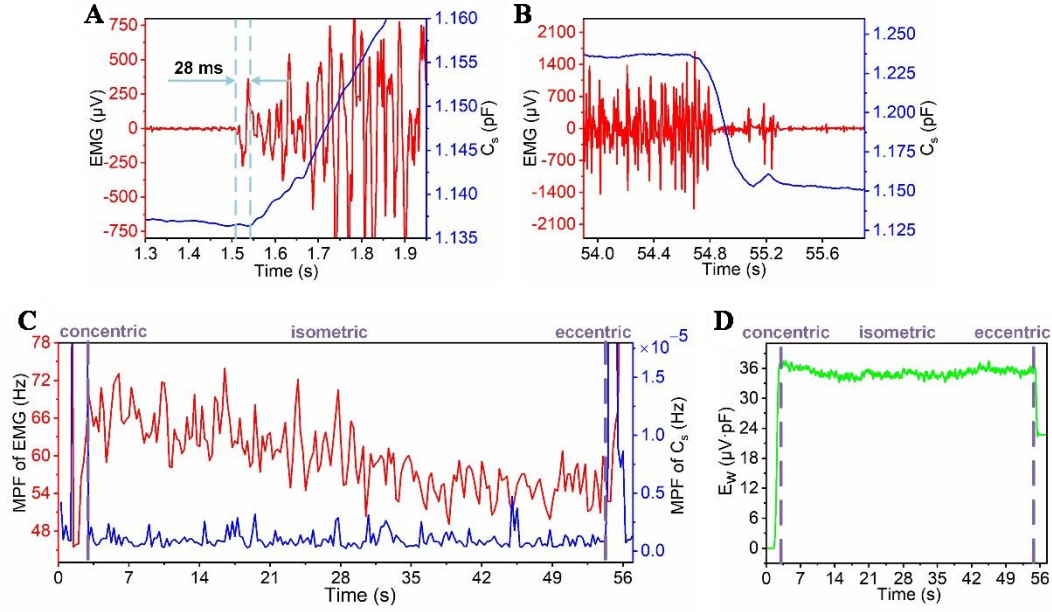
Jiajie Guo^{1,2,*}, Yiran Tong², Chuxuan Guo², Zijie Liu², Hao Yin², Yuchao Liu², Zhuo Li³, Hao Wu², Caihua Xiong^{1,2}

¹Institute of Medical Equipment Science and Engineering, Huazhong University of Science and Technology, Wuhan 430074, Hubei, China.

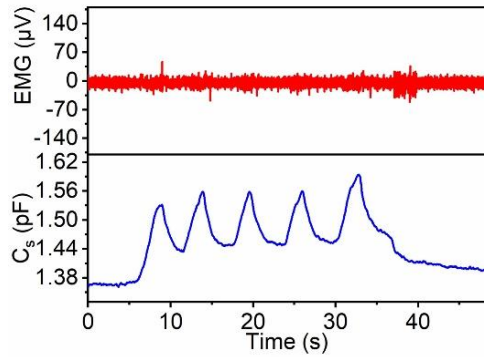
²State Key Laboratory of Intelligent Manufacturing Equipment and Technology, School of Mechanical Science and Engineering, Huazhong University of Science and Technology, Wuhan 430074, Hubei, China.

³Department of Materials Science and State Key Laboratory of Molecular Engineering of Polymers, Fudan University, Shanghai 200433, China.

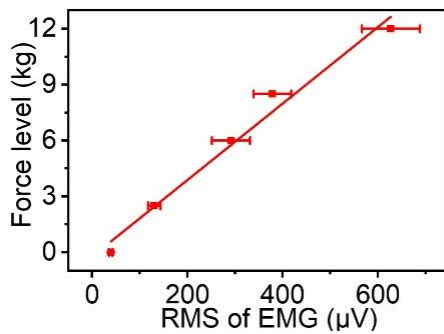
***Correspondence to:** Prof. Jiajie Guo, Institute of Medical Equipment Science and Engineering, Huazhong University of Science and Technology, 1037 Luoyu Road, Hongshan District, Wuhan 430074, Hubei, China. E-mail: jiajie.guo@hust.edu.cn



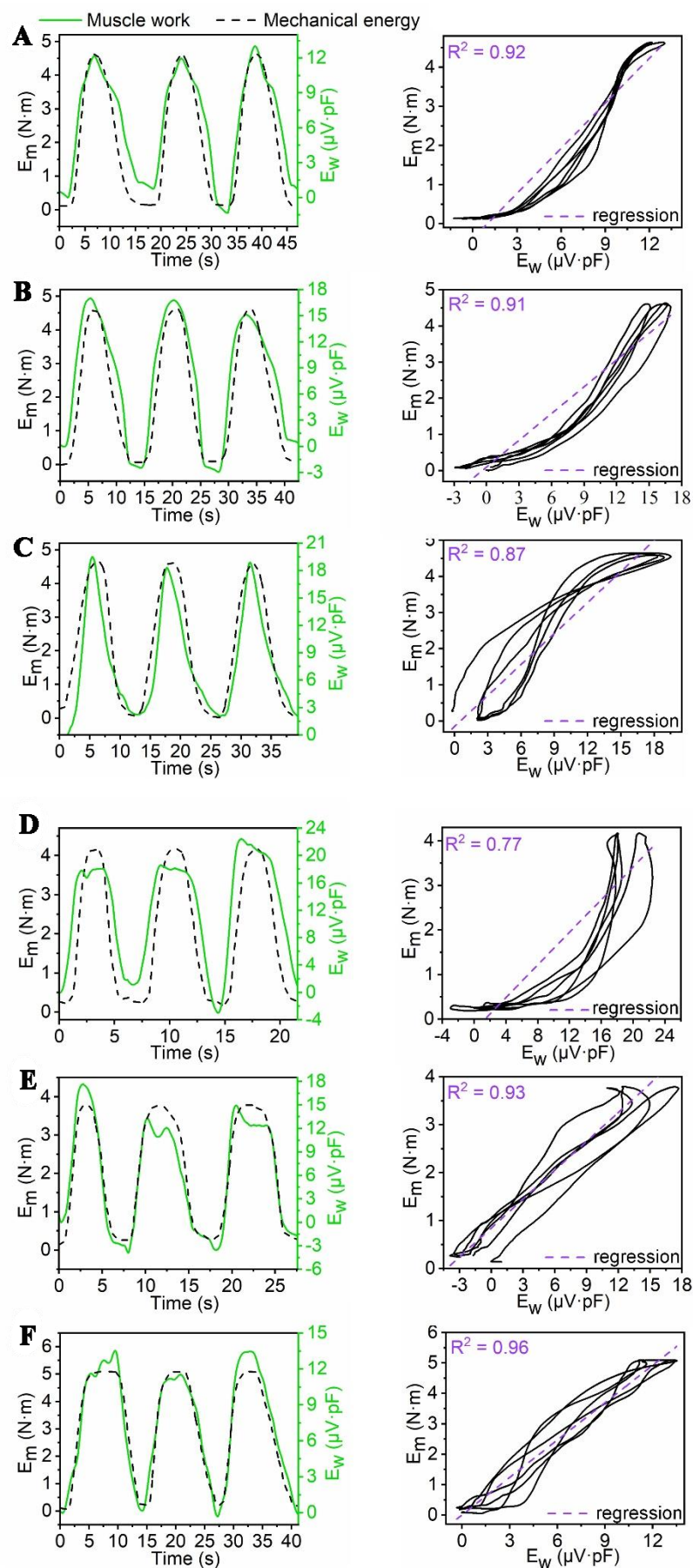
Supplementary Figure 1. Characterization of the measured EMG and capacitive deformation for concentric, eccentric and isometric muscle contractions. (A) Time difference between the measured EMG and the capacitive deformation. The measured EMG occurred approximately 28 ms earlier than the muscle deformation; (B) Measured EMG and capacitive deformation during passive stretching. The measured EMG vanished during the muscle eccentric contraction when the muscle relaxed with passive stretching by the holding weight; (C) Frequency features of the measured EMG and capacitive deformation. The MPF, calculated with the Fast Fourier Transform (FFT), was employed to characterize the muscle signals. The MPF of the EMG gradually decreased by 31.8% during isometric contraction due to muscle fatigue, while the MPF of C_s stayed about zero as the muscle did not deform during quasi-static holding of the weight; (D) Variations of E_w during muscle fatigue. The E_w calculated using Eq. (1) increased during concentric muscle contraction, remained constant during isometric muscle contraction, and slightly decreased during the eccentric contraction by passive stretching. During isometric contraction, E_w stayed constant as the muscle performed little work. However, the muscle still needed to consume metabolic energy to maintain muscle tensions as well as basic biological processes which would lead to fatigue during prolong holding of the weight.



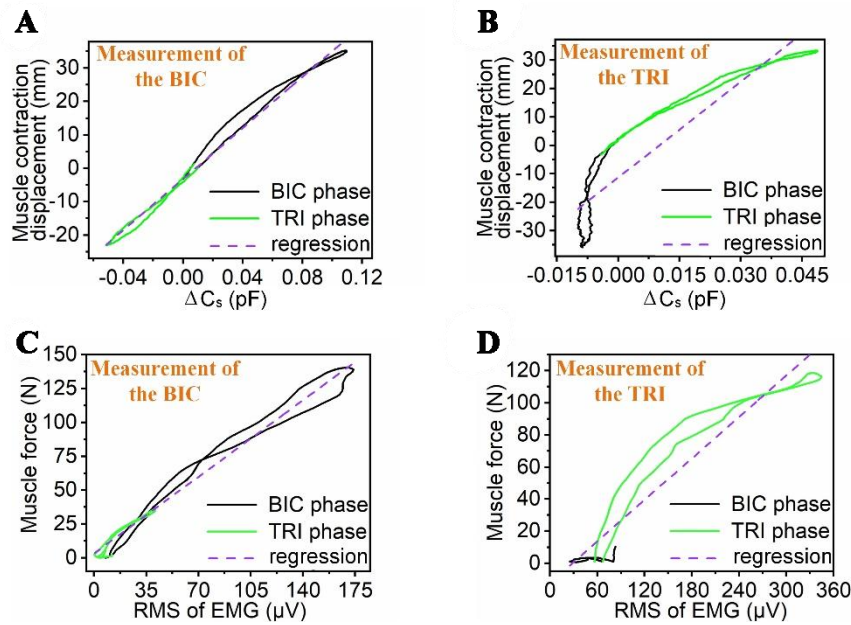
Supplementary Figure 2. Neural-mechanical sensing for passive compression on a muscle. A stable interfacial impedance was achieved to eliminate artifacts of the measured EMG during muscle motions, where the neural-mechanical sensor was secured by the double-sided foam adhesive and preloaded with non-stretchable fabric tapes on the skin. When the muscle was gently pressed and passively deformed by five times, the attached sensor detected significant mechanical deformations without EMG variation. This observation demonstrates that EMG sensing does not interfere with muscle deformations.



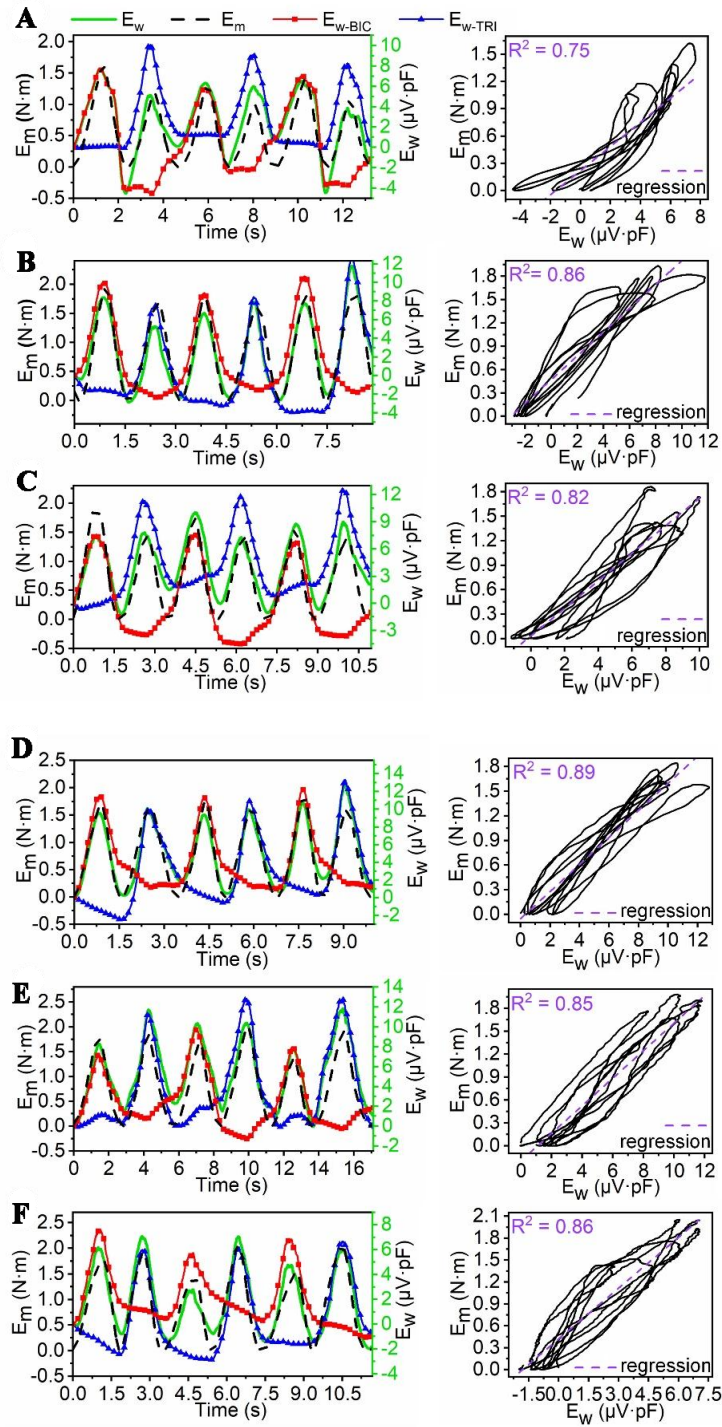
Supplementary Figure 3. Linear relationship between the RMS of EMG and muscle force levels. The measured EMG for different force levels was assessed with isometric muscle contractions in tests of static-holding different weights. The RMS of EMG was calculated using the data sample and lasted for three seconds. Their linear relationship is quantified by the R^2 exceeding 0.97, justifying the representation of muscle force with RMS of EMG.



Supplementary Figure 4. Robustness of performed work sensing for a single muscle. Each sub-figure illustrates results of one healthy volunteer in the weight lifting test. The muscle work performed by the BIC muscles exhibited a similar variation as the mechanical energy of the weight (left column). Linear regression of the muscle work and mechanical energy was characterized by R^2 with an average value of 0.88 (right column).



Supplementary Figure 5. Calibration of muscle deformation and muscle force sensing. (A and B) Linear regression of the contraction displacement with the change of C_s . It is observed that the change of C_s matches with the muscle contraction displacement via $R^2 = 0.98$ and 0.85 for the BIC and TRI muscles, respectively. It validates the assumption that displacement of muscle contraction is linear with change of the measured C_s for collaborative muscle motions; (C and D) Relationship between RMS of EMG and muscle contraction force. The RMS of EMG matches with the muscle force via linear regression of $R^2 = 0.98$ and 0.91 for the BIC and TRI muscles, respectively. It validates the assumption that RMS of EMG is proportional to the muscle force during collaborative muscle motions.



Supplementary Figure 6. Sensing robustness of effective work performed by multiple muscles. Each sub-figure illustrates results of one subject out of six healthy volunteers in the weight lifting test involving both BIC and TRI muscles. Summation of muscle work individually done by the BIC (red line for E_{w-BIC}) and TRI (red line for E_{w-TRI}) produces the total muscle work E_w , and it is consistent with the change in mechanical energy E_m of the weight (left column). The linear regression of E_m with E_w is characterized by R^2 with an average value of approximately 0.83 (right column).

Supplementary Note 1. Dynamic analysis of the weight lifting motions.

In the case of weight lifting (Supplementary Figure 7), the angle γ ranges from -13° to $90^\circ/-36^\circ$ to -90° , during which the BIC provides contraction force, and the TRI is in a passively stretched state. Conversely, in the case of multiple muscle lifting (Supplementary Figure 7B), the situation is reversed at $\gamma = -90^\circ$ to -144° . L_{11} and L_{12} denote the lengths of humerus and radius (ulna) bones, and (L_{21}, α_1) and (L_{22}, α_2) characterize the attachment positions of BIC and TRI on the radius and ulna, respectively; θ denotes the orientation of the upper arm with respect to the horizontal X axis, γ is the rotation angle of the forearm.

The muscle length is estimated as

$$L_i = \sqrt{L_{11}^2 + L_{2i}^2 - 2L_{11}L_{2i}\cos(\theta - \alpha_i - \gamma)} \quad (\text{A1})$$

where $i = 1$ for the BIC and $i = 2$ for the TRI, respectively, and their differentials with respect to γ are given by

$$\Delta L_i = -L_{11} \cdot L_{2i} \sin(\theta - \alpha_i - \gamma) \cdot \Delta\gamma / \sqrt{L_{11}^2 + L_{2i}^2 - 2L_{11} \cdot L_{2i} \cos(\theta - \alpha_i - \gamma)} \quad (\text{A2})$$

The lateral displacement of muscle deformation is given as

$$\Delta X_i = \mu X_i \frac{\Delta L_i}{L_i} \quad (\text{A3})$$

where L_i and X_i represent the axial and lateral dimensions of the muscle at the undeformed state, respectively, and Poisson's ratio μ is 0.5 for an incompressible muscle tissue. It has been calibrated by ultrasound imaging that the muscle lateral deformation ΔX_i is proportional to the measured capacitance change ΔC_s via the coefficient k_c . The above leads to the relation between muscle deformation displacement ΔL_i and the capacitance change ΔC_s

$$\Delta L_i = k_1 \Delta C_s \quad (\text{A4})$$

where $k_1 = L_i k_c / (\mu X_i)$. Calculate ΔL_i for different orientations of the forearm γ using (B2). The above linear relation between ΔL_i and ΔC_s is validated by the single muscle case with $R^2 = 0.92$ for BIC (Figure 4B) and the multiple muscle case with $R^2 = 0.98$ and 0.85 for BIC and TRI, respectively (Supplementary Figure 5A and B).

Since the forearm weight can be negligible compared to the lifted weight, moment equilibrium with respect to the elbow joint is given by

$$F_1 d_1 - F_2 d_2 = mgL_{12} \cos \gamma + mL_{12}^2 \ddot{\gamma} + [k_p |\cos \gamma| + (k_{b1} - k_{b2})] |(\gamma + \gamma_c)| \quad (A5)$$

where $\ddot{\gamma}$ is the angular acceleration of the forearm rotation, $k_p |(\gamma + \gamma_c) \cos \gamma|$ and

$(k_{b1} - k_{b2}) |(\gamma + \gamma_c)|$ are active and passive antagonistic torque of the muscle when it is

stretched, the arm length of the muscle with respect to the elbow joint is

$d_i = L_{11} L_{2i} \sin(\theta - \alpha_i - \gamma) / L_i$, and F_i represents the contraction forces with $i = 1$ for BIC

and $i = 2$ for TRI, respectively. For the case with only BIC working (Supplementary

Figure 7A), and TRI is passive; for the case with both BIC and TRI (Supplementary

Figure 7B), the active BIC and passive TRI produce the elbow rotation for $-36^\circ \leq \gamma \leq -90^\circ$, the passive BIC and active TRI drive the elbow rotation for $-90^\circ < \gamma \leq -144^\circ$. In

this way, each muscle force F_i is given by

$$F_i = \begin{cases} (-1)^{i-1} mL_{12} (g \cos \gamma + \ddot{\gamma} L_{12}) / d_i + k_{bi} |(\gamma + \gamma_c)| / d_i & \text{for active contraction} \\ [(-1)^{i-1} k_p |\cos \gamma| / d_i + k_{bi} / d_i] |(\gamma + \gamma_c)| & \text{for passive elongation} \end{cases} \quad (A6)$$

The relationship between the muscle force F and RMS of EMG U_R has been established in the previous study

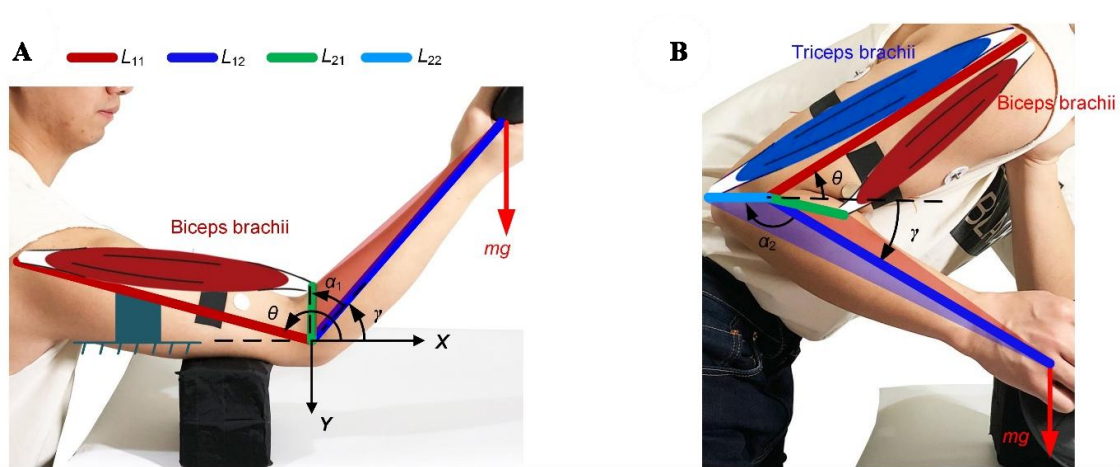
$$F = k_2 U_R \quad (A7)$$

Calculate F for different orientations of the forearm γ using (A6). The above linear

relation between muscle force and RMS of EMG is validated by the single muscle case

with $R^2 = 0.9$ for BIC (Figure 4D) and the multiple muscle case with $R^2 = 0.98$ and 0.91

for BIC and TRI, respectively (Supplementary Figure 5C and D).



Supplementary Figure 7. Weight lifting tests with one single muscle and multiple muscle coordination.

Supplementary Table 1. Comparison with existing techniques related to energy sensing

	Softness	Wearable	In-situ sensing	Sensing rate (Hz)	Measurements	Applications
Metabolic energy analyzer ^[1, 2]		√		0.5~1	Carbon dioxide concentration	Metabolic cost assessment
Near-infrared spectroscopy ^[3-5]		√	√	2	Hemoglobin concentration	oxygen saturation detection
Isotonic testing system ^[6, 7]				200	Force and acceleration	Muscle power sensing
EMG and Inertial Measuring Unit ^[8, 9]		√		100~400	EMG and acceleration	Motion pattern recognition
Coupled neural-mechanical sensor	√	√	√	100	EMG and deformations	Muscle work monitoring

Supplementary Table 2. Comparison with existing wearable sensing methods

Monitoring Method	Advantages	Disadvantages
Traditional Surface EMG	<ol style="list-style-type: none">1. Real-time neural activation monitoring2. Non-invasive, cost-effective ^[10]	<ol style="list-style-type: none">1. Inability to distinguish between active contraction, passive deformation, and static force generation mechanisms.^[11]2. Lack of a direct method to quantify the mechanical work output of individual muscles.
Ultrasound Imaging	<ol style="list-style-type: none">1. Visualization of soft tissue deformations^[12]2. Monitoring of local muscle morphology	<ol style="list-style-type: none">1. Requirement of complex image processing algorithms ^[13]2. Lack of real-time in-situ monitoring capability3. High equipment cost
Optical Motion Capture	<ol style="list-style-type: none">1. High-precision kinematic analysis ^[14]2. Facilitation of multi-joint synergy modeling	<ol style="list-style-type: none">1. Dependence on inverse dynamic models that leads to error propagation ^[15]2. Lack of real-time in-situ monitoring3. Intensive computation ^[16]
Our Bimodal Sensor	<ol style="list-style-type: none">1. Simultaneous EMG and capacitive displacement sensing (shared electrodes)2. Real-time in-situ monitoring of individual muscle work3. Independence on complex physiological or kinematic models	<ol style="list-style-type: none">1. Current version is insufficient for whole-body muscle synergy analysis, which requires sensor network development.2. Limited sensitivity for deep muscle monitoring

References

1. D. J. Macfarlane, P. Wong: Validity, reliability and stability of the portable Cortex Metamax 3B gas analysis system. *European Journal of Applied Physiology* 112, 2539-2547 (2012).
2. S. Kolmogorov, A. Vorontsov, J. P. Vilas-Boas: Metabolic Power, Active Drag, Mechanical and Propelling Efficiency of Elite Swimmers at 100 Meter Events in Different Competitive Swimming Techniques. *Applied Sciences-Basel* 11, 14 (2021).
3. S. Perrey, V. Quaresima, M. Ferrari: Muscle oximetry in sports science: an updated systematic review. *Sports Medicine* 54, 975-996 (2024).
4. T. Scheeren, P. Schober, L. Schwarte: Monitoring tissue oxygenation by near infrared spectroscopy (NIRS): background and current applications. *J. Clin. Monit. Comput.* 26, 279-287 (2012).
5. A. Scano, I. Pirovano, M. E. Manunza, L. Spinelli, D. Contini, A. Torricelli, R. Re: Sustained fatigue assessment during isometric exercises with time-domain near infrared spectroscopy and surface electromyography signals. *Biomedical Optics Express* 11, 7357-7375 (2020).
6. R. J. Schmitz, K. C. Westwood: Knee extensor electromyographic activity-to-work ratio is greater with isotonic than isokinetic contractions. *J. Athl. Train.* 36, 384 (2001). <https://pmc.ncbi.nlm.nih.gov/articles/PMC155433/>
7. T. Kojima: Force-velocity relationship of human elbow flexors in voluntary isotonic contraction under heavy loads. *Int. J. Sports Med.* 12, 208-213 (1991). 10.1055/s-2007-1024669
8. J. Lopes, M. Simão, N. Mendes, M. Safeea, J. Afonso, P. Neto: Hand/arm gesture segmentation by motion using IMU and EMG sensing. *Procedia Manuf.* 11, 107-113 (2017). 10.1016/j.promfg.2017.07.158
9. S. Jiang, B. Lv, W. Guo, C. Zhang, H. Wang, X. Sheng, P. B. Shull: Feasibility of wrist-worn, real-time hand, and surface gesture recognition via sEMG and IMU sensing. *IEEE Trans. Ind. Inform.* 14, 3376-3385 (2017). 10.1109/TII.2017.2779814
10. M. Al-Ayyad, H. A. Owida, R. De Fazio, B. Al-Naami, P. Visconti: Electromyography monitoring systems in rehabilitation: A review of clinical applications, wearable devices and signal acquisition methodologies. *Electronics* 12, 1520 (2023).
11. A. Rainoldi, T. Moritani, G. Boccia: EMG in exercise physiology and sports.

Surface electromyography: Physiology, engineering, and applications, 501-539 (2016).

12. A. S. Sahrman, L. Vosse, T. Siebert, G. G. Handsfield, O. Röhrle: Determination of muscle shape deformations of the tibialis anterior during dynamic contractions using 3D ultrasound. *Frontiers in Bioengineering and Biotechnology* 12, 1388907 (2024).

13. H. J. Hu, H. Huang, M. H. Li, X. X. Gao, L. Yin, R. X. Qi, R. S. Wu, X. J. Chen, Y. X. Ma, K. R. Shi, C. H. Li: A wearable cardiac ultrasound imager. *Nature* 613, 23 (2023).

14. Y. Lee, B. Lama, S. Joo, J. Kwon: Enhancing Human Key Point Identification: A Comparative Study of the High-Resolution VICON Dataset and COCO Dataset Using BPNET. *Applied Sciences-Basel* 14, 19 (2024).

15. H. P. H. Shum, E. S. L. Ho, Y. Jiang, S. Takagi: Real-Time Posture Reconstruction for Microsoft Kinect. *IEEE Transactions on Cybernetics* 43, 1357-1369 (2013).

16. M. Hatamzadeh, L. Busé, F. Chorin, P. Alliez, J. D. Favreau, R. Zory: A kinematic-geometric model based on ankles' depth trajectory in frontal plane for gait analysis using a single RGB-D camera. *J. Biomech.* 145, 7 (2022).